ISSN 1392–1320 MATERIALS SCIENCE (MEDŽIAGOTYRA). Vol. XX, No. X. 2024

Analysis of Friction Stir Welded Joint Properties of 2A12 Aluminum Alloy

Xiaole GE [1, 2, 3], Hongfeng WANG [1, 2, 3] *, Da HUANG [2, 3], Weiwei SONG [1, 2, 3]

[1] *College of Mechanical and Electrical Engineering, Huangshan University, Huangshan, China*
[2] *Anhui Tea-Chrysanthemum Intelligent Processing Equipment Engineering Research Center, Huangshan University, Huangshan, China*
[3] *Huangshan Technology Innovation Center of Friction Stir Welding, Huangshan University, Huangshan, China*

http://doi.org/10.5755/j02.ms.34723

Received 27 July 2023; accepted 6 November 2023

2A12 hot-rolled aluminum alloy has high plasticity and toughness, and is widely used in the manufacturing of structural parts in aviation, aerospace, automobiles, and other fields. To explore the effect of friction stir welding process parameters on the welded joint properties of 2A12 hot-rolled aluminum alloy, experimental investigations were conducted. The surface appearance of the welded joints under different process parameters was observed, the microstructure, microhardness, tensile strength, yield strength, elongation and the fracture morphology of the welded joints were assessed. The findings suggested that when the rotation speed was 600 rpm and the forward speed was 250 mm/min, the tensile strength, yield strength and elongation of the welded joint were all maximum, which were 437.6 MPa, 381.6 MPa and 7.5 % respectively, reaching 85.5 %, 88.1 % and 35.7 % of the base material. Under the same forward speed, the tensile strength and elongation of the welded joint initially rose and subsequently declined with the increment of rotation speed. The microhardness distribution of the welded joint exhibited a W-shape pattern. The fracture morphology showed that the fracture type of the welded joint was a ductile fracture. Unlike the base material, the welded joints did not exhibit significant necking during the tensile testing. The research results can be utilized as a reference for the engineering application of friction stir welding of 2A12 hot-rolled aluminum alloy.
Keywords: 2A12 aluminum alloy, FSW, microstructure, mechanical properties.

1. INTRODUCTION

Due to its lightweight, high strength, and excellent corrosion resistance, aluminum alloys have been extensively applied in diverse industries such as automotive, watercraft, and aerospace. 2A12 aluminum alloy is known for its high fracture toughness, corrosion resistance, good plasticity and machinability [1]. It can be utilized in components such as aircraft fuselages, automotive body structures, high-speed train shells, and ship decks. In engineering applications, it is often necessary to join multiple aluminum alloy plates together to form a cohesive structure. Traditional fusion welding methods, due to the occurrence of imperfections like heat cracks, voids, and oxide inclusions in the welding procedure, are not suitable for welding 2A12 aluminum alloy [2, 3, 4]. The emergence of friction stir welding (FSW) has offered a viable solution for achieving excellent welding of 2A12 aluminum alloy. FSW is a solid state joining technique that was developed by The Welding Institute of the United Kingdom in 1991 [5]. It eliminates the requirement for welding consumables and gas protection, offers fast welding speed, and no pollution to the environment [6]. FSW can be applied to the welding of various materials, such as aluminum alloys [7], titanium alloys [8], magnesium alloys [9, 10], copper alloys [11], and steels [12].

The research on FSW of aluminum alloys has evolved from conventional butt welding to various forms such as lap welding, pinless welding, and ultrasonic-assisted welding [13]. Guo et al. explored the impact of different FSW process parameters on the dynamic fracture characteristics of welded joint (WJ) in 2024 and 7075 aluminum alloys. The study revealed that the yield strength within the heat-affected zone (HAZ) was superior to that in the stirring zone (SZ) and thermo-mechanically affected zone (TMAZ), and the fracture mode of the joints was ductile and transgranular fracture [14]. Additionally, Guo et al. studied the residual stress distribution in WJ of 2024 and 7075 aluminum alloys [15]. Fu et al. analyzed the influence of thermal input and subsequent aging after welding on the hardness of the WJ in 2024 aluminum alloy thin plates. The research indicated that thermal input had a notable effect on the hardness of the WJ, while the aging after welding had a limited impact on the improvement of the hardness in the WJ [16]. Khajeh et al. investigated the mechanical and electrical properties of WJs between 2024 aluminum alloy and copper dissimilar materials. The study analyzed the formation mechanism of the microstructure in the SZ and found that under certain conditions of the ratio of tool rotation speed to tool forward speed, abundant intermetallic compounds and defects were formed in the WJs, which adversely affected the tensile strength and resistivity [17]. Deng et al. investigated the impact of the zinc brazing interface on the microstructure and mechanical properties of friction stir lap WJs between 2A12 aluminum alloy and AZ31 magnesium alloy. The research indicated that the zinc brazing interface expanded the area of the lap joint, and improved its mechanical properties to some extent [5]. Xuan et al. explored the impact of the shape of the tool pin on the interface

* Corresponding author. Tel.: +86-19805590556.
E-mail: *105092@hsu.edu.cn* (H. F. Wang)

imperfections in friction stir lap WJs of 2A12 aluminum alloy. The formation mechanism of the interface imperfections was analyzed through numerical simulation. It was found that a conical pin could create a uniform and continuous velocity field and withstand the maximum failure load [13]. Liu et al. designed four different groove-distributed pinless FSW tools and studied the WJ properties of 2A12 aluminum alloy under different tools. The research revealed that the six-groove tool achieved the best material plastic flow and maximum tensile strength [1]. Furthermore, Hu et al. investigated the WJ properties of 2219 aluminum alloy using ultrasonic vibration assisted FSW. The study revealed the effect of ultrasonic vibration on the microstructure and mechanical properties of WJs. Under the action of ultrasonic vibration, the hardness distribution of the WJ became more uniform, the dislocation density and residual stress decreased, and the tensile strength increased [18].

The 2A12 hot-rolled aluminum alloy has good mechanical properties, especially excellent plasticity, and crack resistance at high temperatures. Presently, there is more extensive research on FSW of 2 series aluminum alloy, with relatively less attention directed towards 2A12 hot-rolled aluminum alloy. Due to the special forming processes associated with 2A12 hot-rolled aluminum alloy, the scope of the FSW process for this material differs from that of other 2 series aluminum alloys. Therefore, there is a need for the investigation of the FSW process for 2A12 hot-rolled aluminum alloy. This work aims to investigate the effect of FSW process parameters on the WJ properties of 2A12 hot-rolled aluminum alloy. To achieve this goal, six groups of FSW experiments were conducted. The microstructure and mechanical properties of the WJs under various process parameters were tested, and the fracture morphology of the WJs was explored. The research findings can promote a more profound understanding of the FSW process of 2A12 hot-rolled aluminum alloy and provide references for selecting FSW process parameters of 2A12 hot-rolled aluminum alloy.

2. MATERIALS AND METHODS

5 mm thick 2A12 hot-rolled aluminum alloy plates with dimensions of 200 (length) × 60 (width) mm were utilized for conducting FSW experiments. The chemical compositions (wt.%) of 2A12 aluminum alloy are: Si0.5, Cu3.8-4.9, Mg1.2-1.8, Zn0.3, Mn0.3-0.9, Ti0.15, Ni0.1, Fe0.5, bal. Al. The FSW experiments were performed using an FSW machine produced by Beijing FSW Technology Co., Ltd. and a self-made tool with a material of H13 steel. The pin of the tool has a conical shape with diameters of 4.6 mm and 6.6 mm. The length of the pin was 4.9 mm. The end surface of the tool is processed with grooves. The tool shoulder has a diameter of 18 mm. The tool tilt angle during the FSW process was set to 0.5°. The schematic diagram of FSW of 2A12 aluminum alloy in this study is shown in Fig. 1.

Six groups of process parameters were set up for FSW experiments, as listed in Table 1. The surface appearance of the welded joints under different process parameters was observed using a 3D digital microscope. The microstructure test samples, microhardness test samples, and tensile test samples were fabricated by using a wire cutting machine provided by Suzhou Hanqi CNC Equipment Co., Ltd.

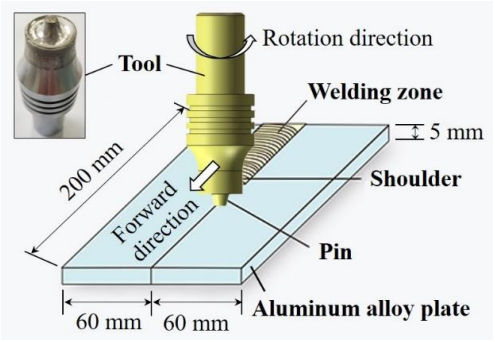

Fig. 1. Schematic diagram of FSW of 2A12 aluminum alloy

Table 1. FSW process parameter configurations

Group number, GN	Rotation speed, rpm	Forward speed, mm/min
GN 1	500	200
GN 2	600	200
GN 3	700	200
GN 4	500	250
GN 5	600	250
GN 6	700	250

Before microstructure observation, the observation surface was initially ground using metallographic sandpapers. After the observation surface was ground to a smooth condition, a polishing machine was employed to eliminate any remaining scratches. Subsequently, the polished observation surface was etched with Keller's reagent for approximately 8 seconds. Finally, the observation surface was thoroughly cleaned using anhydrous alcohol. The microstructure distribution in different zones of the WJs at the cross section was observed using a metallographic microscope manufactured by Suzhou Yueshi Precision Instrument Co., Ltd.

Before conducting microhardness testing, the test surface was initially ground using metallographic sandpapers. When the test surface was ground to a smooth state, a polishing machine was used for polishing. The microhardness of the WJs at the cross section was tested using a Vickers hardness tester, and the location and distribution of the test points are shown in Fig. 2. The applied pressure during microhardness testing was 0.3 kg, with a holding time of 10 s. The tensile strength of the WJs under various process parameters was tested using a tensile testing machine with a stretching rate of 1 mm/min. The fracture morphology of the WJs was observed with a scanning electron microscope.

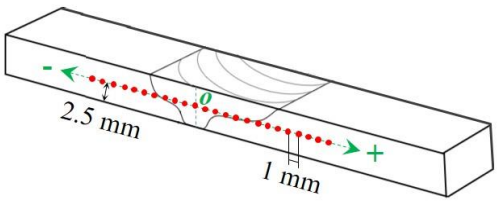

Fig. 2. Schematic diagram of microhardness testing

3. RESULTS AND DISCUSSION

3.1. Surface appearance

The surface appearance of the WJs under different process parameters is shown in Fig. 3. As presented in Fig. 3, the surfaces of the WJs are relatively smooth without any visible pore defects, indicating good surface formation quality within the range of process parameters. However, slight burrs are present at the boundaries of the WJs. Although the presence of these burrs might not have an obvious impact on the usability of the WJs, it is customary to apply additional post-weld processing techniques, such as milling and polishing, to achieve the desired surface quality after FSW. This additional step ensures that the weld seam meets the necessary standards and meets the requirements for its intended application.

Fig. 3. Surface appearance of the WJs under different process parameters: a – GN 1; b – GN 2, c – GN 3; d – GN 4; e – GN 5; f – GN 6

The height profile waveforms of the WJ surface under different process parameters are depicted in Fig. 4.

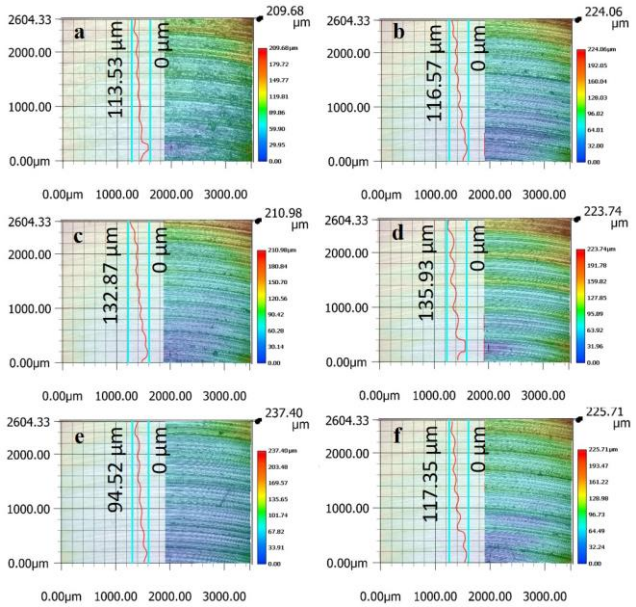

Fig. 4. Height profile waveforms of the WJ surface under different process parameters: a – GN 1; b – GN 2; c – GN 3; d – GN 4; e – GN 5; f – GN 6

The height profile waveform can characterize the surface flatness of the WJs, where a smaller fluctuation amplitude in the waveform indicates better surface flatness. As observed in Fig. 4, GN 4 exhibits the highest maximum height profile value of 135.93 μm, which indicates a slightly less uniform surface flatness compared to other process parameters. This is primarily attributed to the lower heat input associated with these process parameters (low rotation speed and high forward speed). Consequently, the material experiences less softening during the welding process, leading to non-uniform material flow in the welding zone. This non-uniform material flow results in more pronounced processing patterns on the weld surface and reduced surface flatness. Moreover, GN 5 has the lowest maximum height profile value of 94.52 μm, suggesting a smoother and more consistent surface. This may be because the heat input under this process parameter is relatively reasonable, and the material can obtain a stable flow state during the welding process, resulting in a comparatively smoother surface after welding. However, when evaluating the overall results, there is relatively little variation in the maximum height profile values of the WJ surfaces, indicating a stable surface flatness of the WJs across various process parameters.

3.2. Microstructure

The microstructure of the base material is shown in Fig. 5. As depicted in Fig. 5, the cross section of the base material exhibits elongated grains with relatively large sizes. This is primarily attributed to the distribution of grains along the rolling direction during the hot rolling process of the base material. As a result, the grains take on this elongated shape. In addition, it can be observed that the microstructure distribution at various cross-sectional locations is relatively uniform, which is one of the main factors for the good mechanical properties of the base material.

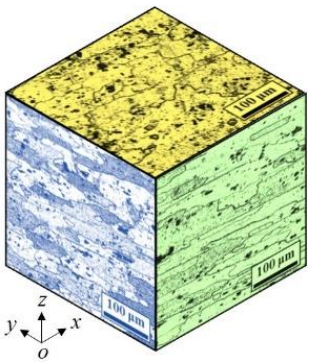

Fig. 5. Microstructure distribution of base material at different cross sections

The microstructure of a typical WJ is shown in Fig. 6. From Fig. 6, it can be observed that the cross-sectional morphology of the WJ of 2A12 aluminum alloy can be categorized into distinct regions: the stirring zone (SZ), thermo-mechanically affected zone (TMAZ), heat-affected zone (HAZ), and base material zone (BMZ). The SZ undergoes dynamic recrystallization and experiences significant grain refinement owing to the intensive stirring of the tool and the elevated temperature [19]. In the TMAZ, the grains exhibit an elongated shape resulting from shear stress and deformation by plasticity [14]. Since the heat input in TMAZ is limited and the plastic

deformation of the material is also small, there is no recrystallization of the grains in this zone [20]. The HAZ is primarily influenced by high temperature without obvious plastic deformation, resulting in coarser grains compared to the BMZ [21, 22]. The BMZ, experiencing minimal temperature and deformation, shows no significant change in grain structure. It is noteworthy that the boundary of SZ and TMAZ is clearer on the advancing side compared to the retreating side, and the variation in grain size is more pronounced. This is largely due to the higher shear stress and temperature experienced by the material on the advancing side, leading to more noticeable plastic flow [23]. The clear boundary on the advancing side was also observed in the study of [1].

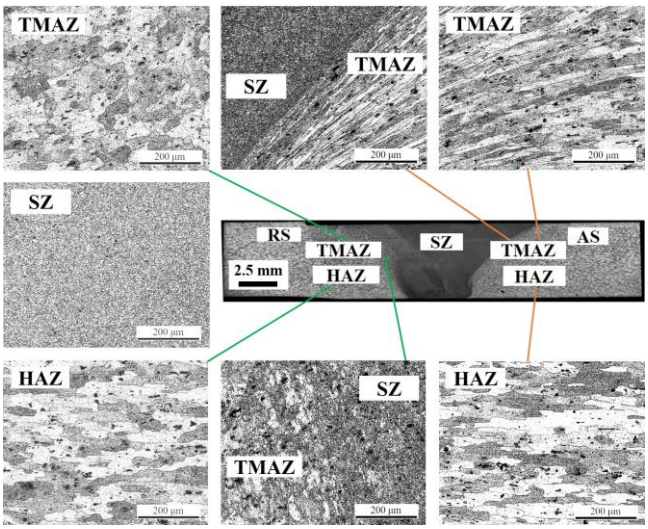

Fig. 6. Microstructure distribution in different zones of the WJ of GN 5 at the cross section

The microstructure of the SZ of the WJ under various process parameters is shown in Fig. 7.

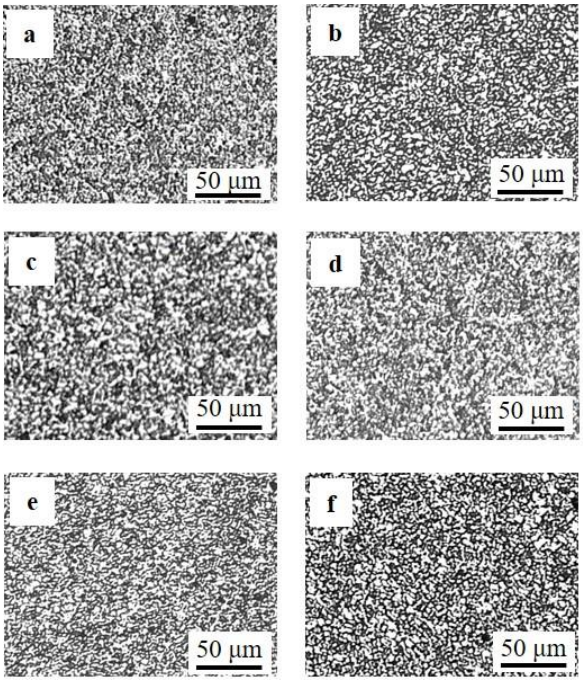

Fig. 7. Microstructure of the SZ of the WJ under various process parameters: a – GN 1; b – GN 2; c – GN 3; d – GN 4; e – GN 5; f – GN 6

Fig. 7 shows that the grains in the SZ are relatively small under various FSW process parameters. This is attributed to the occurrence of dynamic recrystallization in the SZ under high temperature and severe plastic deformation, resulting in the formation of uniformly fine grains [24]. As rotation speed gradually increases, there is a tendency for the grains in the SZ to become larger. This phenomenon can be primarily attributed to the higher temperature in the SZ at higher rotation speeds, which promotes grain growth in the SZ. Nevertheless, with an increase of forward speed, the grains in the SZ tend to decrease in size. This behavior can be explained by the effect of forward speed on the temperature distribution in the welding area. A faster forward speed results in a shorter duration of high-temperature exposure in the SZ. As a result, the thermal energy is applied for a shorter time, impeding the rapid growth of grains and leading to smaller grain sizes.

3.3. Microhardness

The microhardness of base material and microhardness distribution curves of the WJs under different process parameters at the cross-section are shown in Fig. 8.

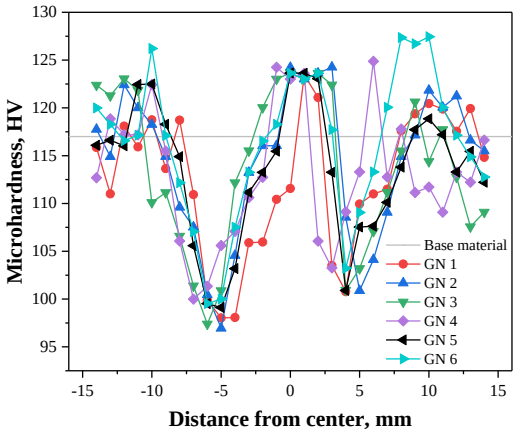

Fig. 8. Microhardness of base material and microhardness distribution curves of the WJs under different process parameters at the cross-section

It can be observed from Fig. 8 that the microhardness distribution at the WJ exhibits a typical W-shape. The lowest microhardness value is found near the HAZ [16], while the highest microhardness value within the WJ is located in the SZ and exceeds the microhardness of the base material. This notable difference in microhardness is principally because of the variations in grain structure between these two regions. The SZ possesses a finer grain structure due to the generation of sufficient dynamic recrystallization, contributing to its enhanced microhardness [25], while the HAZ contains coarser grains under the influence of frictional heat, resulting in a lower microhardness value. As the test point moves from the BMZ to the HAZ, the microhardness gradually reduces due to the increase in grain size [21]. From the HAZ to the TMAZ, the microhardness gradually increases. This is because the TMAZ has finer grains than HAZ, and the combined effect of mechanical stirring and frictional heat increases the dislocation density in this zone [1], resulting in increased microhardness. Overall, there is not a significant difference in microhardness among the SZ,

TMAZ and HAZ of the WJ under various process parameters.

3.4. Tensile strength

The stress-strain curves and elongation of WJs under various process parameters are shown in Fig. 9. From Fig. 9, it is evident that the elongation of the base material is relatively high, reaching 21.0 %, whereas the elongation of the WJs is significantly lower than that of the base material. The reason for this phenomenon is mainly related to the non-uniform microstructure and microhardness in the WJs [9, 26]. It can be seen from Fig. 6 and Fig. 8 that there are significant differences in microstructure and microhardness in the SZ, TMAZ, and HAZ. Such non-uniformity in microstructure and microhardness reduces the plasticity and elongation of the WJs. Additionally, during the welding process, the generation of residual stresses within the WJs, owing to elevated temperatures and high stress levels, renders the WJs more susceptible to fracture under loading conditions, thereby diminishing the elongation [27, 28]. From another perspective, it is noteworthy that the elongation of the WJs varies significantly under different process parameters. When the rotation speed is 600 rpm and the forward speed is 250 mm/min (GN5), the maximum elongation of 7.5 % is achieved. In contrast, with a rotation speed of 700 rpm and a forward speed of 200 mm/min (GN3), the minimum elongation is observed, merely amounting to 1.5 %. Furthermore, the base material exhibits a distinct necking phenomenon at the fracture location, while such a necking phenomenon is not evident in the friction stir welded samples under different process parameters. This is consistent with the variation in elongation.

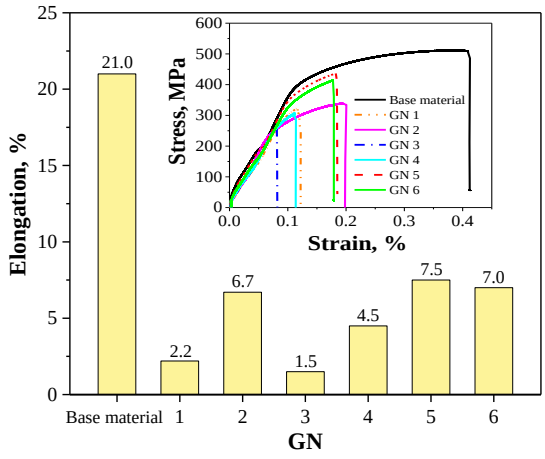

Fig. 9. Stress-strain curves and elongation of WJs under various process parameters

The tensile strength and yield strength of WJs under various process parameters are shown in Fig. 10. From Fig. 10, it can be observed that the tensile strength and yield strength of the base material are both the highest, measuring 511.6 MPa and 433.2 MPa, respectively. In contrast, the WJs exhibit lower tensile strength and yield strength when compared to those of the base material. Specifically, at a rotation speed of 600 rpm and a forward speed of 250 mm/min (GN 5), the tensile strength and yield strength of WJs are the highest, which are 437.6 MPa and 381.6 MPa respectively, reaching 85.5 % and 88.1 % of the base material respectively. This shows that under these process parameters, the materials of the upper plate and the lower plate can be well mixed, which helps to form better metallurgical performance [29]. When the rotation speed is 700 rpm and the forward speed is 200 mm/min (GN 3), the WJs exhibits the lowest tensile strength and yield strength, representing only 51.1 % and 53.3 % of the base material. This can be attributed to the increased heat input during welding under high rotation speed and low forward speed conditions, resulting in excessive coarsening of the microstructure within the WJ, thereby reducing the joint strength [30]. This indicates that the strength of the WJ of 2A12 aluminum alloy is sensitive to process parameters, and inappropriate process parameters will result in lower welding strength.

Furthermore, as evident from Fig. 9 and Fig. 10, at the same forward speed, with the gradual increase in rotation speed, elongation and tensile strength exhibit a consistent trend of initially increasing and subsequently decreasing. Consequently, it can be deduced that excessively high or low rotation speeds are detrimental to the enhancement of WJ strength and elongation. Additionally, it was observed during the experiment that the fracture locations of most samples under various process parameters were near the TMAZ and the HAZ, aligning with the results in [14]. This is mainly because strength weaknesses are easily formed near TMAZ and HAZ with uneven microstructure, and microcracks are easily generated under the action of residual stress, causing the WJ to break from near TMAZ and HAZ [31, 32].

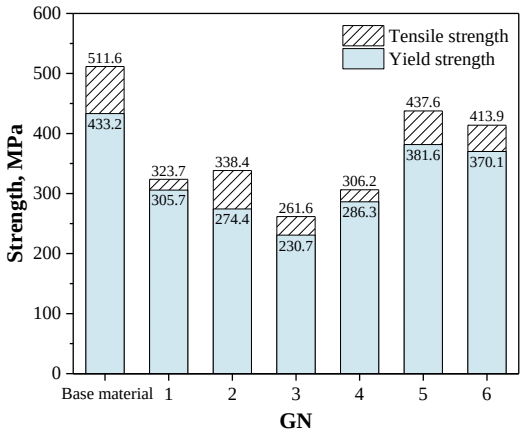

Fig. 10. Tensile strength and yield strength of WJs under various process parameters

3.5. Fracture morphology

Fig. 11 presents the morphology of the tensile fracture surfaces under typical process parameters. It can be observed from Fig. 11 that there are distinct tear ridges and numerous dimples at the fracture surface, which are typical characteristics of ductile fracture [33]. This indicates that the fracture type of the WJ of 2A12 aluminum alloy is a ductile fracture. In comparison to the fracture morphology of WJs, the dimples in the base material fracture surface are larger and deeper, indicating excellent plasticity and toughness of the base material. This is also a significant reason for the pronounced necking phenomenon observed in the base material sample. Furthermore, the fracture pattern of the base material exhibits a 45° shear fracture.

The dimple distribution under the process parameters of GN 3 (high rotation speed and low forward speed) is uneven, which may be caused by uneven bonding of materials in WJ. Under this condition, the welding zone experiences excessive temperature due to the long contact time between the tool and the material, leading to severe material plasticization and recrystallization grain recovery [15, 29], which reduces the bonding effect between the upper plate and the lower plate to a certain extent. In comparison to GN 3, the distribution of dimples in GN 5 is more closely packed, which provides the basis for a high-strength WJ.

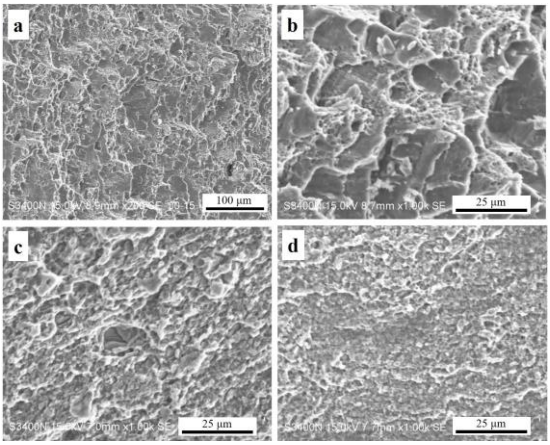

Fig. 11. Morphology of the tensile fracture surfaces under typical process parameters: a, b – base material; c – GN 3; d – GN 5

4. CONCLUSIONS

At a rotation speed of 600 rpm and a forward speed of 250 mm/min, the tensile strength, yield strength and elongation of the welded joint were all maximum, which were 437.6 MPa, 381.6 MPa and 7.5 % respectively, reaching 85.5 %, 88.1 % and 35.7 % of the base material. Under the same forward speed, the tensile strength and elongation of the welded joint showed a trend of initially increasing and then decreasing as the rotation speed gradually increased. Within the selected range of process parameters, good surface formation quality can be achieved. The fracture morphology of the welded joint indicated ductile fracture, with the main fracture locations near the HAZ and the TMAZ. Compared to the base material, the welded joint did not exhibit significant necking during the tensile process.

Acknowledgments

The authors gratefully acknowledge the financial support from the Key Research Project of Natural Science in Anhui Higher Education Institutions (No. 2022AH051947), the Key Research and Development Project in Anhui Province (No. 202104b11020011), the Excellent Scientific Research and Innovation Team of Universities in Anhui Province (No. 2022AH010103), the Major Science and Technology Project of Anhui Province (No. GXXT-2021-06) and the Research Project of Huangshan University (No. hsxyssd006).

REFERENCES

1. **Liu, Z.L., Cui, H.T., Ji, S.D., Xu, M.Q., Meng, X.C.** Improving Joint Features and Mechanical Properties of Pinless Friction Stir Welding of Alcald 2A12-T4 Aluminum Alloy *Journal of Materials Science & Technology* 32 (12) 2016: pp. 1372 – 1377. https://doi.org/10.1016/j.jmst.2016.07.003
2. **Li, G.H., Zhou, L., Luo, L.Y., Wu, X.M., Guo, N.** Microstructural Evolution and Mechanical Properties of Refill Friction Stir Spot Welded Alclad 2A12-T4 Aluminum Alloy *Journal of Materials Research and Technology* 8 (5) 2019: pp. 4115 – 4129. https://doi.org/10.1016/j.jmrt.2019.07.021
3. **Li, J.N., Su, M.L., Qi, W.J., Wang, C., Zhao, P., Ni, F., Liu, K.G.** Mechanical Property and Characterization of 7A04-T6 Aluminum Alloys Bonded by Friction Stir Welding *Journal of Manufacturing Processes* 52 2020: pp. 263 – 269. https://doi.org/10.1016/j.jmapro.2020.02.018
4. **Qian, S.H., Zhang, T.M., Chen, Y.H., Xie, J.L., Chen, Y., Lin, T.S., Li, H.X.** Effect of Ultrasonic Impact Treatment on Microstructure and Corrosion Behavior of Friction Stir Welding Joints of 2219 Aluminum Alloy *Journal of Materials Research and Technology* 18 2022: pp. 1631 – 1642. https://doi.org/10.1016/j.jmrt.2022.03.068
5. **Deng, H.B., Chen, Y.H., Zhang, T.M., Wang, S.L., Yin, L.M., Xie, J.L.** Effect of Zn-brazed-interface on Microstructures and Mechanical Properties of Dissimilar 2A12/AZ31 Alloys Friction Stir Lap Welds *Materials Letters* 255 2019: pp. 126543. https://doi.org/10.1016/j.matlet.2019.126543
6. **Anil Kumar, H.M., Venakata Ramana, V., Shanmuganathan, S.P.** Experimental Investigation of Mechanical Properties and Morphological Studies on Friction Stir Welded Aluminum 2024 Alloy *Materials Today: Proceedings* 5 (1) 2018: pp. 700 – 708. https://doi.org/10.1016/j.matpr.2017.11.136
7. **Yang, Y., Bi, J., Liu, H.W., Li, Y., Li, M.Y., Ao, S.S., Luo, Z.** Research Progress on the Microstructure and Mechanical Properties of Friction Stir Welded Al-Li Alloy Joints *Journal of Manufacturing Processes* 82 2022: pp. 230 – 244. https://doi.org/10.1016/j.jmapro.2022.07.067
8. **Zhang, Z., Tan, Z.J., Wang, Y.F., Ren, D.X., Li, J.Y.** The Relationship Between Microstructures and Mechanical Properties in Friction Stir Lap Welding of Titanium Alloy *Materials Chemistry and Physics* 296 2023: pp. 127251. https://doi.org/10.1016/j.matchemphys.2022.127251
9. **Xie, L.W., Xiao, X., Zhu, X.Y., Fan, Y.X., Jiang, C., Song, Y.L.** Influence Mechanism of Pin Thread in Friction Stir Welding of Magnesium Alloys Based on the Relationship Between Microstructure and Mechanical Properties *Journal of Materials Processing Technology* 312 2023: pp. 117870. https://doi.org/10.1016/j.jmatprotec.2023.117870
10. **Xu, N., Ren, Z.K., Lu, Z.D., Shen, J., Song, Q., Zhao, J.H., Bao, Y.F.** Improved Microstructure and Mechanical Properties of Friction Stir-welded AZ61 Mg Alloy Joint *Journal of Materials Research and Technology* 18 2022: pp. 2608 – 2619. https://doi.org/10.1016/j.jmrt.2022.03.160
11. **You, J.Q., Zhao, Y.Q., Dong, C.L., Miao, S., Liu, Z., Liu, Li., Su, Y.H.** Microstructural Evolution and Mechanical Properties of the Al-Cu Dissimilar Joint Enhanced by Stationary-dynamic Shoulder Friction Stir

Welding *Journal of Materials Processing Technology* 300 2022: pp. 117402.
https://doi.org/10.1016/j.jmatprotec.2021.117402

12. **Zhang, T., Wang, K.S., Qiao, K., Wu, B., Liu, Q., Han, P., Wang, W., Wang, Y.Y., Hao, Z.Y., Zheng, P.F.** Evolution Mechanism of Intermetallic Compounds and the Mechanical Properties of Dissimilar Friction Stir Welded QP980 Steel and 6061 Aluminum Alloy *Materials Characterization* 202 2023: pp. 113033.
https://doi.org/10.1016/j.matchar.2023.113033
13. **Xiao, X., Qin, D.Q., Mao, Y., Fu, L.** Effects of Pin Morphology on the Interface Defects of the FSWed Lap Joints of 2A12 Aluminum Alloy *Journal of Manufacturing Processes* 68 2021: pp. 128 – 140.
https://doi.org/10.1016/j.jmapro.2021.05.023
14. **Guo, Y.N., Ma, Y., Wang, F.** Dynamic Fracture Properties of 2024-T3 and 7075-T6 Aluminum Friction Stir Welded Joints with Different Welding Parameters *Theoretical and Applied Fracture Mechanics* 104 2019: pp. 102372.
https://doi.org/10.1016/j.tafmec.2019.102372
15. **Guo, Y.N., Ma, Y., Zhang, X.S., Qian, X.D., Li, J.** Study on Residual Stress Distribution of 2024-T3 and 7075-T6 Aluminum Dissimilar Friction Stir Welded Joints *Engineering Failure Analysis* 118 2020: pp. 104911.
https://doi.org/10.1016/j.engfailanal.2020.104911
16. **Fu, R.D., Zhang, J.F., Li, Y.J., Kang, J., Liu, H.J., Zhang, F.C.** Effect of Welding Heat Input and Post-welding Natural Aging on Hardness of Stir Zone for Friction Stir-welded 2024-T3 Aluminum Alloy Thin-sheet *Materials Science and Engineering: A* 559 2013: pp. 319 – 324.
https://doi.org/10.1016/j.msea.2012.08.105
17. **Khajeh, R., Jafarian, H.R., Seyedein, S.H., Jabraeili, R., Eivani, A.R., Park, N., Kim, Y., Heidarzadeh, A.** Microstructure, Mechanical and Electrical Properties of Dissimilar Friction Stir Welded 2024 Aluminum Alloy and Copper Joints *Journal of Materials Research and Technology* 14 2021: pp. 1945 – 1957.
https://doi.org/10.1016/j.jmrt.2021.07.058
18. **Hu, Y.Y., Liu, H.J., Fujii, H.** Improving the Mechanical Properties of 2219-T6 Aluminum Alloy Joints by Ultrasonic Vibrations During Friction Stir Welding *Journal of Materials Processing Technology* 271 2019: pp. 75 – 84.
https://doi.org/10.1016/j.jmatprotec.2019.03.013
19. **Li, J.Q., Liu, H.J.** Effects of the Reversely Rotating Assisted Shoulder on Microstructures During the Reverse Dual-rotation Friction Stir Welding *Journal of Materials Science & Technology* 31 (4) 2015: pp. 375 – 383.
https://doi.org/10.1016/j.jmst.2014.07.020
20. **Scialpi, A., Filippis, L.A.C.D., Cavaliere, P.** Influence of Shoulder Geometry on Microstructure and Mechanical Properties of Friction Stir Welded 6082 Aluminium Alloy *Materials & Design* 28 (4) 2007: pp. 1124 – 1129.
https://doi.org/10.1016/j.matdes.2006.01.031
21. **Zhao, Y.X., Yang, Z.Y., Domblesky, J.P., Han, J.M., Li, Z.Q., Liu, X.L.** Investigation of Through Thickness Microstructure and Mechanical Properties in Friction Stir Welded 7N01 Aluminum Alloy Plate *Materials Science and Engineering: A* 760 2019: pp. 316 – 327.
https://doi.org/10.1016/j.msea.2019.06.014
22. **Sashank, J.S., Sampath, P., Krishna, P.S., Sagar, R., Venukumar, S., Muthukumaran, S.** Effects of Friction Stir Welding on Microstructure and Mechanical Properties of 6063 Aluminium Alloy *Materials Today: Proceedings* 5 (2) 2018: pp. 8348 – 8353.
https://doi.org/10.1016/j.matpr.2017.11.527
23. **Li, D.X., Yang, X.Q., Cui, L., He, F.Z., Shen, H.** Effect of Welding Parameters on Microstructure and Mechanical Properties of AA6061-T6 Butt Welded Joints by Stationary Shoulder Friction Stir Welding *Materials & Design* 64 2014: pp. 251 – 260.
https://doi.org/10.1016/j.matdes.2014.07.046
24. **Hamiton, C., Dymek, S., Blicharski, M.** A Model of Material Flow during Friction Stir Welding *Materials Characterization* 59 (9) 2008: pp. 1206 – 1214.
https://doi.org/10.1016/j.matchar.2007.10.002
25. **Rajendran, C., Srinivasan, K., Balasubramanian, V., Balaji, H., Selvaraj, P.** Feasibility Study of FSW, LBW and TIG Joining Process to Fabricate Light Combat Aircraft Structure *International Journal of Lightweight Materials and Manufacture* 4 (4) 2021: pp. 480 – 490.
https://doi.org/10.1016/j.ijlmm.2021.07.001
26. **Zhang, L., Zhong, H.L., Li, S.C., Zhao, H.J., Chen, J.Q., Qi, L.** Microstructure, Mechanical Properties and Fatigue Crack Growth Behavior of Friction Stir Welded Joint of 6061-T6 Aluminum Alloy *International Journal of Fatigue* 135 2020: pp. 105556.
https://doi.org/10.1016/j.ijfatigue.2020.105556
27. **Buglioni, L., Tufaro, L.N., Svoboda, H.G.** Thermal Cycles and Residual Stresses in FSW of Aluminum Alloys: Experimental Measurements and Numerical Models *Procedia Materials Science* 9 2015: pp. 87 – 96.
https://doi.org/10.1016/j.mspro.2015.04.011
28. **Fratini, L., Macaluso, G., Pasta, S.** Residual Stresses and FCP Prediction in FSW through a Continuous FE Model *Journal of Materials Processing Technology* 209 2009: pp. 5465 – 5474.
https://doi.org/10.1016/j.jmatprotec.2009.05.001
29. **Anandan, B., Manikandan, M.** Effect of Welding Speeds on the Metallurgical and Mechanical Property Characterization of Friction Stir Welding Between Dissimilar Aerospace Grade 7050 T7651-2014A T6 Aluminium Alloys *Materials Today Communications* 35 2023: pp. 106246.
https://doi.org/10.1016/j.mtcomm.2023.106246
30. **Shi, M., Wang, J.L., Wang, H.F.** Analysis on Microstructures and Mechanical Properties of FSW Joint of 6061 Aluminum Alloy Thin Sheet *Hot Working Technology* 49 (19) 2020: pp. 30 – 34.
https://doi.org/10.14158/j.cnki.1001-3814.20190259
31. **Sabari, S.S., Malarvizhi, S., Balasubramanian, V.** Characteristics of FSW and UWFSW Joints of AA2519-T87 Aluminium Alloy: Effect of Tool Rotation Speed *Journal of Manufacturing Processes* 22 2016: pp. 278 – 289.
https://doi.org/10.1016/j.jmapro.2016.03.014
32. **Salih, O.S., Ou, H., Sun, W.** Heat Generation, Plastic Deformation and Residual Stresses in Friction Stir Welding of Aluminium Alloy *International Journal of Mechanical Sciences* 238 2023: pp. 107827.
https://doi.org/10.1016/j.ijmecsci.2022.107827
33. **Guo, N., Fu, Y.L., Wang, Y.Z., Meng, Q., Zhu, Y.X.** Microstructure and Mechanical Properties in Friction Stir Welded 5A06 Aluminum Alloy Thick Plate *Materials & Design* 113 2017: pp. 273 – 283.
https://doi.org/10.1016/j.matdes.2016.10.030